Available online at www.sciencedirect.com
SCIENCE DIRECT®
Physica B 357 (2005) 45–52
PHYSICA B
www.elsevier.com/locate/physb

Coherence experiments using white synchrotron radiation

Ullrich Pietsch[a,*], Tobias Panzner[a], Wolfram Leitenberger[a], Ivan Vartanyants[b]

[a]*Institute of Physics, University of Potsdam, Am Neuen Palais 10, D-14469 Potsdam, Germany*
[b]*HASYLAB at DESY, D-22603 Hamburg, Germany*

Abstract

Experiments at the bending magnet beamline at BESSY II (EDR beamline) profit from the excellent coherence properties of third generation synchrotron sources. Considering the exponentially decaying incident spectrum, and because no optical elements are installed except slits and vacuum windows, coherence experiments can be performed between $5\,\mathrm{keV} < E < 15\,\mathrm{keV}$. First, the energy dependence of spatial coherence properties were determined measuring diffraction at single and double pinholes. Next, the coherent white radiation was used to probe the morphology of thin films in reflection geometry. The recorded intensity maps (reflectivity versus sample position) provide speckle patterns which reveal the locally varying sample morphology. Setting the incident angle, α_i, smaller or larger than the critical angle of total external reflection, α_c, one should be able to separate the surface height profile from the subsurface density modulation of a sample. The validity of this approach is verified at the example of reciprocal space maps taken from a polymer surface where we could reconstruct the lateral height profile from speckle data.

PACS: 07.85.Qe; 42.25.Kb; 61.10.Kw; 68.35. Md; 82.35.Gh

Keywords: Synchrotron radiation; Coherence; X-ray reflectivity; Polymer surface morphology

1. Introduction

For about 4 years the University of Potsdam has run a bending magnet beamline at the third generation synchrotron source BESSY II at Berlin (Germany) exploiting the hard X-ray part of white synchrotron radiation [1]. Due to the emission spectrum of 1.7 GeV storage ring, the experiments can use a small part of the spectrum only decaying exponentially between $5\,\mathrm{keV} < E < 25\,\mathrm{keV}$. The beamline provides excellent coherent X-ray radiation since no optical elements are installed except slits and vacuum windows. Several experiments were already performed profiting from the continuous spectrum. For example, X-ray reflectivity was used to measure negative thermal expansion of thin polymer films [2,3]. By recording out-of-plane reflectivity and in-plane diffraction

*Corresponding author. Tel.: +49 331 977 1286; fax: 49 33 977 1133.
E-mail address: upietsch@rz.uni-potsdam.de (U. Pietsch).

0921-4526/$ - see front matter © 2004 Elsevier B.V. All rights reserved.
doi:10.1016/j.physb.2004.11.017

simultaneously using two energy-dispersive detectors, we could observe thermally induced phase transitions in organic supramolecular films with a time resolution of a few seconds [4]. Further applications for material characterisation are white beam topography and white beam X-ray fluorescence.

Recently, we started experiments making use of a spatial coherence length of a few tens of microns of the white beam. From our first considerations it was clear from the beginning, that despite the low-energy resolution of an energy-dispersive solid-state detector of about 200 eV, interference phenomena should be observable. Indeed, diffraction patterns have been detected simultaneously in the energy range between $5\,\mathrm{keV} < E < 15\,\mathrm{keV}$ behind single pinholes of different diameters and double pinholes with different separations [5,6,12]. These experiments were used to probe the coherence properties of the beamline and the interface properties of organic thin films in reflectivity geometry.

Coherence experiments to reconstruct the surface morphology of solids were already performed using monochromatic radiation [7,8]. Illuminating a sample with coherent radiation, the scattering pattern can be interpreted by the Fourier transformation of the particular height distribution within the coherently illuminated sample area. In particular, the diffuse scattering splits into speckles which reflects the height fluctuations of the sample on micrometer length scale. Subsequently, the speckle pattern can be used to reconstruct the surface morphology [9]. Despite the low-energy resolution of the energy-dispersive detector and the restricted space within the experimental hutch, we came to the conclusion that coherent experiments can also be performed at the energy-dispersive reflectivity (EDR) beamline using a white beam. One essential advantage of an energy-dispersive set-up for these kinds of experiments is that the footprint area at the sample can be kept constant while scanning the reciprocal space and that a wide q_z range is accessible simultaneously. In this paper, we will show that this technique makes it possible to distinguish between surface and sub-surface information recording coherent reflectivity pattern with incident angles α_i smaller or slightly larger than the critical angle of total external reflection, α_c. In particular, we reconstructed the sample morphology of a thin polymer film covered on silicon from the measured speckle pattern.

2. Experiment

The general setup of the experiment is shown in Fig. 1. The incident beam is guided through a 30 m long evacuated tube and is released into air through a 100 μm Kapton window (exit window). The absorber box contains aluminium foils of various thickness to tailor the detectable beam intensity. Next, the beam passes a pinhole at a distance of 0.215 m in front of the sample. The container houses a set of five different pinhole (5–50 μm) diameters made from platinum. The pinholes are adjustable via remote control in

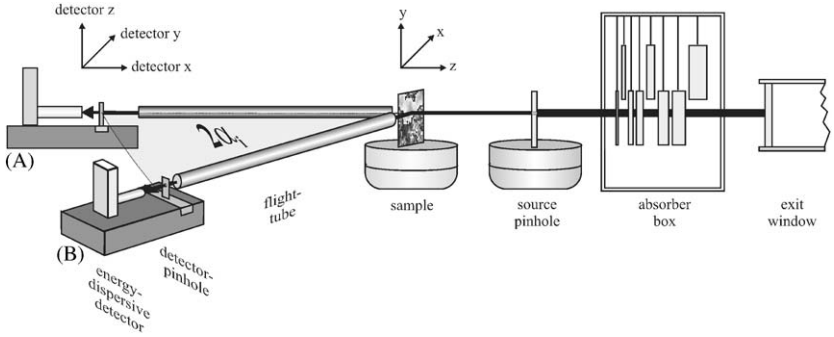

Fig. 1. Experimental set-up for pinhole experiments (position A) and reflectivity measurements with coherent radiation (position B) at the EDR beamline of BESSY II.

the plane perpendicular to the beam direction. In between the sample and energy-dispersive detector an evacuated tube is placed in order to reduce absorption and scattering by air. The effective detector area is restricted by a second pinhole of typically 10 μm in diameter to achieve a good spatial resolution. The spectral distribution of the incident radiation $I(E)$ can be approximated by a function $I(E) = a\exp(-bE)\exp(-c/E^3)$, where $a = 10^7$ cps, $b = 0.5\,\mathrm{keV}^{-1}$ and $c = 400-4000\,\mathrm{keV}^3$ are parameters describing the total intensity through a 10 μm pinhole, the decay of the BESSY emission spectrum and the absorption by air and absorbers, respectively. The lowest detectable energy is limited by air absorption and the maximum energy usable is limited by the exponential decay of the BESSYII spectrum. In summary, one can use a spectral range between $5\,\mathrm{keV} < E < 15\,\mathrm{keV}$ for experiments with coherent radiation. The number of coherent photons is sufficiently large considering the very low noise of the ED detector. The measurements of the intensity distribution of a diffraction pattern using a small detector pinhole requires a large dynamic range of the detector. While in the centre of the diffraction pattern the intensity is extremely high, it decreases strongly with the distance to the centre. Each energy-dispersive experiment suffers from the relatively low integral count number, which can be processed by the detector. The used XFlash 100 (Fa. Roentec [10]) allows to execute an integral count rate of 30 000 cps with only a small loss of linearity of the count rate due to dead time effects and "pile-ups". Due to very low noise of the detector, even very low signals can be measured—they are limited by the "count statistics".

To measure the coherence properties of the beamline we installed the detector directly into the incident beam direction (position A in Fig. 1) and measured diffraction by pinholes with different diameter, i.e. without a sample within the beam path. Here the source-pinhole to detector distance was 1.4 m. The pinhole diffraction was recorded by scanning the detector in a vertical direction through the diffracted beam. Because the intensity of the incident beam is still too high, the detector was offset by a few micrometers horizontally.

For measuring reflectivity, the sample was equippied at a goniometer and illuminated by the incident beam with a fixed incident angle α_i. The detector was moved out horizontally to a scattering angle $\alpha_f = 2\alpha_i$ (position B in Fig. 1). At this geometry, one probes the specularly scattered intensity simultaneously within the accessible energy range. At this fixed scattering geometry, the sample is scanned through the incident beam in the y-direction (sample scan) in order to probe the sample morphology. This has the advantage that the illuminated footprint area is always constant. Using a 10 μm wide beam the vertical step width was 10 μm as well.

An off-set scan can be recorded as well, moving the detector horizontally out of the specular condition by an off-set angle $\Delta\alpha$. Reciprocal space maps are obtained by recording energy spectra at fixed sample position for varying $\Delta\alpha$ and subsequent transformation into reciprocal space using Eq. (1).

$$\begin{aligned} q_x &= \frac{2\pi\cdot E}{\mathrm{hc}}(\cos(\alpha_f)-\cos(\alpha_i)) \\ &\approx -\frac{kE}{2}(\Delta\alpha\cdot\alpha_i), \\ q_z &= \frac{2\pi\cdot E}{\mathrm{hc}}(\sin(\alpha_f)+\sin(\alpha_i)) \\ &\approx \frac{kE}{2}(2\alpha_i+\Delta\alpha), \end{aligned} \tag{1}$$

where $\alpha_f = \alpha_i + \Delta\alpha$ is the extit angle with respect to the sample surface and E is the photon energy in kilo-electron-volt and $k \approx 1.013\,\mathrm{\AA}^{-1}/\mathrm{keV}$ [2,3].

3. Characterization of the incident beam by pinhole experiments

Fig. 2 shows four experimental diffraction patterns recorded using single pinholes with different diameters. The detector pinhole always was 5 μm. Whereas the interference fringes are clearly visible for the 10 and 15 μm pinholes, their contrast decreases for 25 μm and disappears for the 35 μm pinhole. Already from visual inspection, one finds out that the vertical transverse coherence length Λ has to have a value between 25 and 35 μm

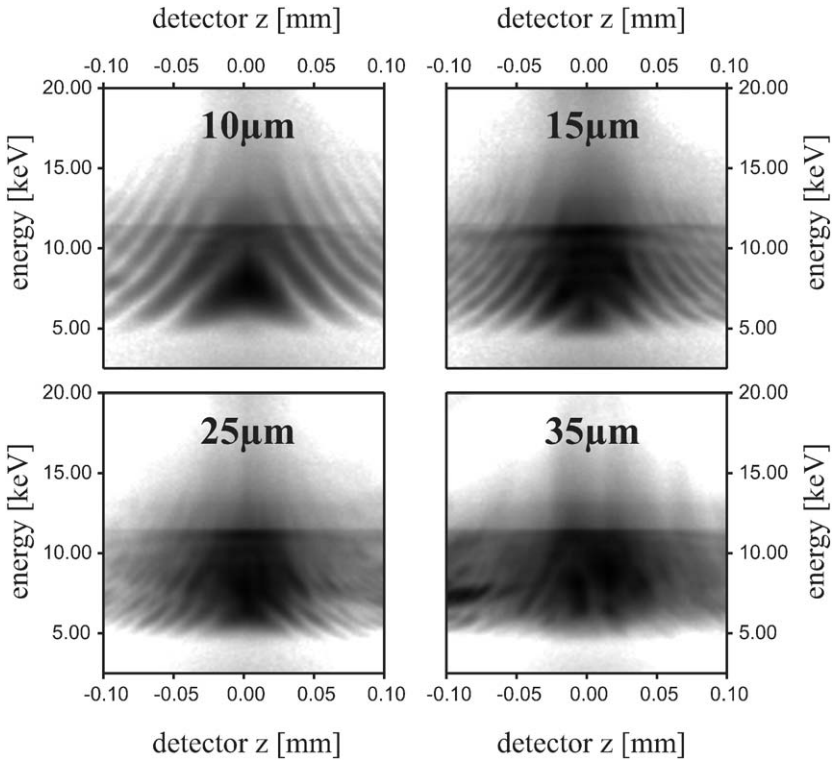

Fig. 2. Fraunhofer diffraction pattern obtained after scattering at a 10, 15, 25 and 35 µm pinhole. From the visibility of fringes one can already see by eye that the transversal coherence length has a value between 25 and 35 µm.

within the accessible spectrum. The straight contrast line at about 12 keV probably marks an absorption edge of detector material. At a certain energy E, and for a pinhole diameter of d, the averaged visibility $V(E)$

$$V(E) = \frac{I_{\max}(E) - I_{\min}(E)}{I_{\max}(E) + I_{\min}(E)} = \left| \frac{\sin\left(\frac{\pi s d E}{12{,}398 R}\right)}{\frac{\pi s d E}{12{,}398 R}} \right| \quad (2)$$

is approximated by the contrast between the minima and maxima of the diffraction pattern. Although the experimental conditions do not fully satisfy the far-field condition, within the accessible energy range $V(E)$ can be approximated fairly well by the Fraunhofer approach shown at the right-hand side of Eq. (2). It contains the source size s and the source-to-pinhole distance R. As seen in Fig. 3, the visibility decreases nearly linearly with

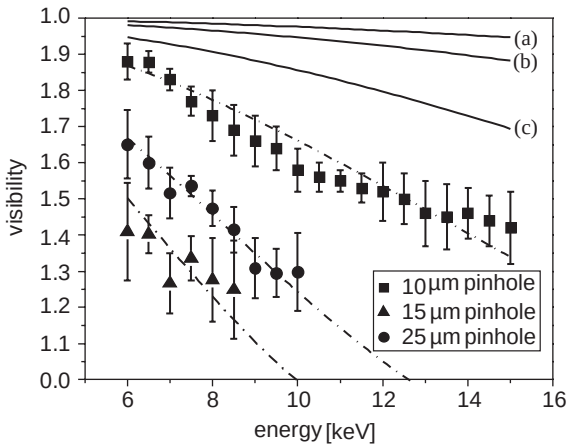

Fig. 3. Energy dependence of the visibility as a function of energy. The black lines show the functional behaviour expected for 10 µm (a), 15 µm (b) and 25 µm (c) using the real geometric parameters s, and R of the beamline. The dotted lines are fits through the data taken from Fig. 2.

increasing energy for all three pinhole diameters used for evaluation. Considering the known source size of a BESSY II bending magnet of $s = 45\,\mu m$ [11] and the real source-pinhole distance $R = 30\,m$ the simulation does not match the experimental data (see black lines in Fig. 3). A reasonable fit one obtains using $s = (46 \pm 6)\,\mu m$ and an effective $R = 7.6\,m$. This R value coincides fairly well with the position of the Be window measured up-stream from the source pinhole, which acts as a "virtual source" [12] for the experiment. The "virtual source" size equals the real source size of the bending magnet.

In general, our experiment has shown that at present experimental conditions a coherent beam experiment with $V > 0.5$ can be realized for pinhole diameters of 10 and 25 μm up to about 16 and 8 keV, respectively.

Qualitatively similar measurements of coherence properties can be performed replacing the single pinhole by two pinholes separated by the certain distance H. As long as H is smaller than Λ, the scattered beams of both pinholes will create the interference pattern of a double slit (Young's experiment) whereas in the opposite case one will find the diffraction pattern of a two neighboured Fraunhofer pattern [13]. That is demonstrated in Fig. 4a, where a 2 μm pinhole were sputtered into a 30 μm thick tantalum foil separated by $H = 37\,\mu m$, respectively. Since Λ is a function of energy, the transition between the two cases appears at a certain energy, here at about 8 keV.

Another possibility of a "double slit" experiment was realized recently using a Fresnel bi-mirror arrangement. It uses the strong demagnification of the length of a mirror if it is observed under very small α_i. In contrast to the experiments made by Fezzaa et al. [14,15] who used two individual mirrors, we used a monolithic version. Two mirror planes of 0.5 mm length at a single wafer were separated by a mechanically milled gap by $H = 7\,mm$. Observing in reflectivity mode under small $\alpha_i = 0.05°$ two thin stripes separated by a few microns act as two point sources and their interference pattern can be observed by a detector at a distance of 1.3 m. The arrangement (see inset in Fig. 4b) acts like Young's double slit experiment. The evaluation of the interference fringes

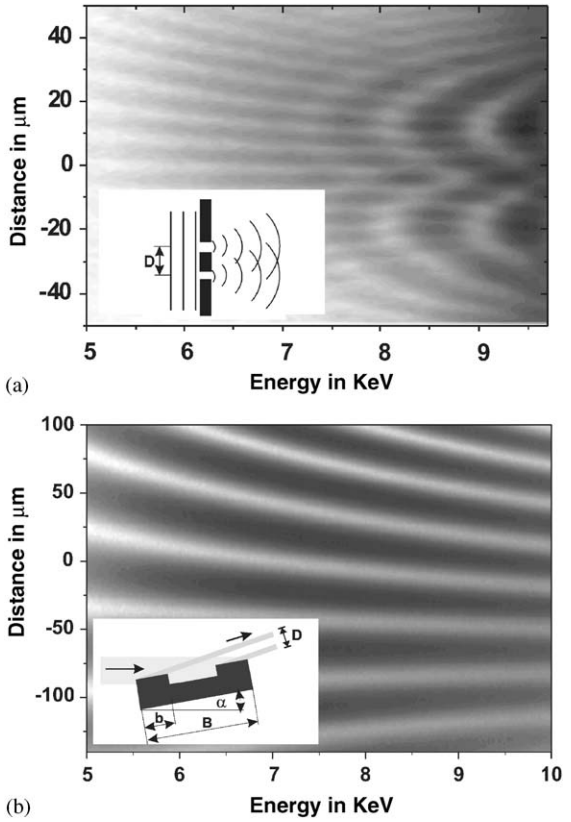

Fig. 4. Double pinhole interference pattern measured in forward direction after scattering at two 2 μm pinhole separated by $H = 37\,\mu m$—Young's slit experiment (a) and after reflection under $\alpha_i = 0.05°$ from two 0.5 mm width mirrors separated $H = 7\,mm$—bi-mirror experiment (b). The respective experimental set-up used is shown as an inset.

can be performed similar to Young's experiment [14,16].

Fig. 4b shows an experimental diffraction pattern measured from a polished silicon wafer. The geometric parameters are equivalent to a Young slit experiment using two slits of 0.9 μm width and 12 μm separation. In contrast to micron sized Young slits for hard X-rays, [12] a millimeter sized bi-mirror is easy to prepare. Additionally, it has the advantage that one can easily change the effective "slit" width and their separation by changing α_i. This device can be used below the angle of total external reflection of the mirror

material without causing problems with unwanted transmission as it happens in the case of a Young experiment using thin metal foils [13]. The experiments show that one can easily determine the degree of coherence of any experimental set-up using a very simple method.

4. Coherent reflectivity from polymer surfaces

The reflectivity of a thin polymer film was probed using the coherent white beam. Using a 10 μm pinhole and for $\alpha_i = 0.152°$, 0.239° and 0.282°, the sample was scanned through the geometrically fixed reflectivity condition in steps $\Delta y = 10\,\mu m$. This is shown in Fig. 5. On increasing α_i an increasing number of thickness oscillations are clearly visible corresponding to an average film thickness of 34 nm. On the other hand, the intensity $I(q_z, y)$ differs strongly for different sample positions y. At a certain y there are additional peaks or any peak at high q_z may exceed the intensity measured at lower q_z-value (see left side of Fig. 5b). This behaviour cannot be understood by specular reflectivity in terms of Fresnel formulas. Here the measured intensity is the Fourier transform of the morphology function $h(x, y)$ of the coherently illuminated sample area, which is 10 μm × 2.4 mm in case of $\alpha_i = 0.239°$.

Interestingly, the reflectivity curve $I(q_z) = \int I(q_z, y)\mathrm{d}y / \int \mathrm{d}y$ behaves like a Fresnel reflectivity multiplied by the spectral function of the incident beam $I(E)$ (see right-hand side of Fig. 5b).

The spatial variation of intensity $I(q_z, y)$ for a certain q_z is accessible in all three intensity patterns of Fig. 5. That means that one and the same q_z has been probed at different α_i. Considering reflection at the air sample interface, the respective particular speckle pattern stems from the surface or from a depth which includes a substantial amount of subsurface information. In Fig. 6 it is clearly seen that the spatial variation of intensity for $\alpha_i = 0.152°$ differs from those extracted at $\alpha_i = 0.239°$; on the other hand the features extracted from 0.239° and 0.289° show a certain similarity.

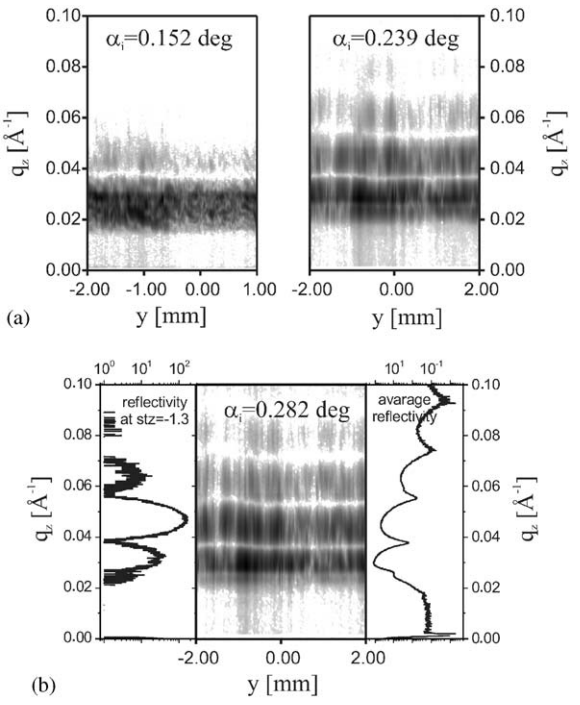

Fig. 5. Sample scans pattern of a thin polymer film recorded at three different α_i. The spatial resolution is 10 μm. The number of visible thickness fringes increases with increasing α_i (a). For $\alpha_i = 0.282°$ (b) we show a single spectrum $I(\alpha_i, y)$ taken at a certain sample position y (left) and the sum spectrum $I(\alpha_i) = \int I(\alpha_i, y)\,\mathrm{d}y$(right).

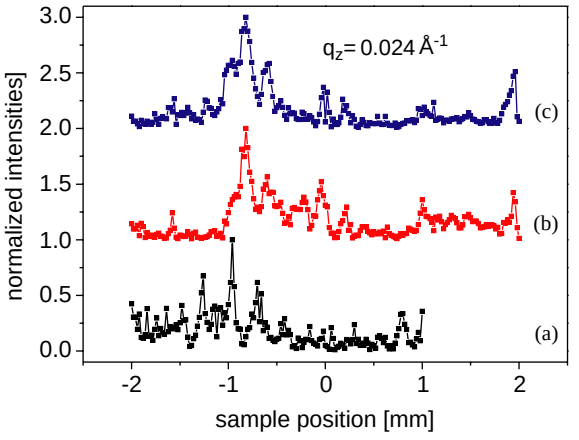

Fig. 6. Line scans extracted for particular q_z-values, but recorded at different α_i. Whereas the features for $\alpha_i = 0.239°$ (b) and 0.289° (c) are similar; they differ from those recorded at $\alpha_i = 0.152°$ (a).

5. Reconstruction of the sample profiles

Sample scans are not sufficient to reconstruct the sample profile $h(x, y)$. It requires an additional lateral momentum transfer q_x. This is realized by recording at series of "off-set scans" with different $\Delta\alpha$ at a particular sample position as shown in Fig. 7a. The respective intensity map $I(E, \Delta\alpha)$ is transformed into a reciprocal space map $I(q_x, q_z)$ (Fig. 7b). It shows distinct features which vary as a function of q_x and q_z. For example, the set of straight lines perpendicular to q_x correspond to a lateral length scale of a few hundred microns. From this reciprocal space map we extracted line scans at certain q_z, which were used to reconstruct the sample profile function. Based on the formalism developed for monochromatic radiation [9] we found the height profile $h(x)$ by iterative fitting of the speckle pattern extracted for a particular q_z. using the relation

$$I(q_x) \approx |A(q_x)|^2, \tag{3a}$$

where $A(q)$ is the speckle amplitude given by

$$A(q_x) \propto F_{\mathrm{CTR}}(q_z) \int_{\Omega} \mathrm{e}^{\mathrm{i}q_z h(x)} \mathrm{e}^{\mathrm{i}(q_x x)}\, \mathrm{d}x, \tag{3b}$$

considering that the resolution in y direction is integrated. In Fig. 3b we neglect the contribution from crystal truncation rod, $F_{\mathrm{ctr}}(q_z)$, which scales with q_z^{-1}. Additionally, we neglect the influence of the polymer substrate interface. The results are

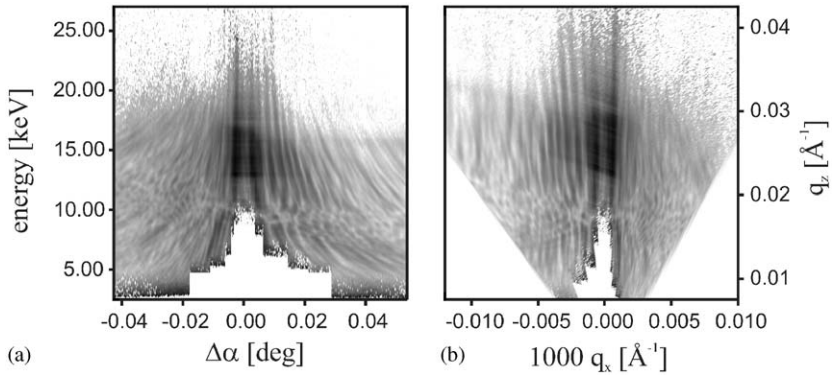

Fig. 7. Reciprocal space map of a polymer sample at a particular sample position. The left figure (a) represents the raw data $I(E, \Delta\alpha)$, obtained by taking several off-set scans with different off-set angle $\Delta\alpha$. The right figure (b) is obtained after transformation into reciprocal space coordinates using Eq. (1).

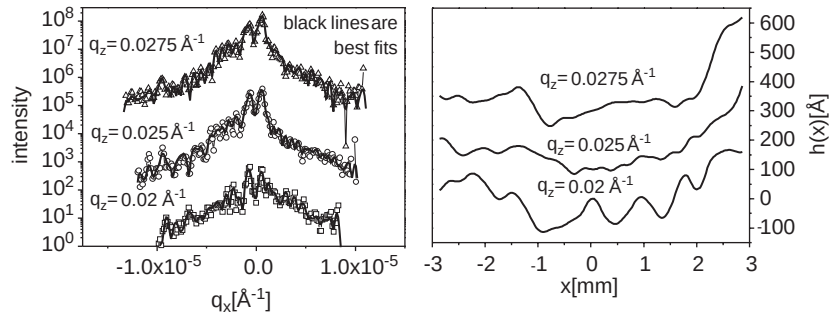

Fig. 8. Results of the fitting procedure of selected line scans taken from Fig. 7b (left graph) and the reconstructed spatial profile (right graph). The lines are vertically displaced. It is seen again, that the pattern for a q_z value smaller than the critical momentum transfer differs significantly from those reconstructed for larger q_z.

shown in Fig. 8 for three different q_z-values. In first approximation we neglect the fact that the energy slightly varies for changing $|q_x|$. At the particular geometric condition and our sample the critical momentum of the film $q_c = 0.021\,\text{Å}^{-1}$. Subsequently $q_z = 0.020\,\text{Å}^{-1}$ probes a sample thickness of 3 nm, whereas the other two q_z values probe a thickness of more than 100 nm. Fig. 8 shows that the morphology changes with q_z. For $q_z < q_c$ the features with a lateral distance of 1.0 mm can be identified with height fluctuations of the films surface, whereas for $q_z > q_c$ they are mainly caused by density fluctuations within the polymer film. In order to separate surface from subsurface information, one has to find an appropriate mechanism to extract both profiles from each other. In the future, the reconstruction method will be applied for dynamic measurements at polymers. For example, it is interesting to observe the melting of artificial surface nanostructures close to the glass transition temperature of the respective polymer [17]. The intrinsic time scale of these processes fits fairly well the experimental possibilities of the EDR beamline.

6. Conclusion

We have demonstrated various tools to characterise the spatial coherence of the radiation of a bending magnet beamline using an energy-dispersive detector. The transverse coherent "white" radiation can be used to probe the morphology of thin films and surfaces. The energy-dispersive method has the advantage that a speckle pattern can be recorded under fixed geometric conditions, which keep the resolution element constant as well. A second advantage is the possibility to probe a certain range of q_z-values simultaneously. This can be used to probe the momentum transfer at conditions below or above the critical momentum of the material under investigation. In general, we have shown that one can Fourier transform the recorded speckle pattern in order to reconstruct the respective morphology function. In the future we are planning to probe surface height fluctuations and subsurface density fluctuations simultaneously. The intensity of the EDR beamline at BESSY II is sufficient to observe temporal fluctuations of speckle pattern on a second time scale.

Acknowledgements

The authors thank BESSY II staff for experimental support and MPI- Colloid & Interface Science (Potsdam- Golm) for financial support.

References

[1] U. Pietsch, J. Grenzer, Th. Geue,, F. Neissendorfer, G. Brezsesinski, Ch. Symietz, H. Möhwald, W. Gudat , Nucl. Instrum. Methods 467–468 (2001) 1077.
[2] M. Mukherjee, M. Bhattacharya, M.K. Sanyal, Th. Geue, J. Grenzer, U. Pietsch, Phys. Rev. E 66 (2002) 061801.
[3] M. Bhattacharya, M. Mukherjee, M.K. Sanyal, Th. Geue, J. Grenzer, U. Pietsch, J. Appl. Phys. 94 (5) (2003) 2882.
[4] Y. Bodenthin, J. Grenzer, R. Lauter, U. Pietsch, P. Lehmann, D.G. Kurth, H. Möhwald, J. Synchrotron. Radiat. 9 (2002) 206.
[5] T. Panzner, W. Leitenberger, J. Grenzer, Y. Bodenthin, Th. Geue, U. Pietsch, H. Möhwald, J. Phys. D: Appl. Phys. 36 (2003) A93.
[6] W. Leitenberger, H. Wendrock, L. Bischoff, T. Panzner, U. Pietsch, J. Grenzer, A. Pucher, Physica B 336 (2003) 63.
[7] I.K. Robinson, J.R. Pindak, R.M. Fleming, S.B. Dierker, K. Ploog, G. Grübel, D.L. Abernathy, J. Als-Nielsen, Phys. Rev. B 52 (1995) 9917.
[8] J.L. Libbert, R. Pindack, S.B. Dierker, I.K. Robinson, Phys. Rev. B 56 (1997) 6454.
[9] I.A. Vartanyants, J.A. Pitney, J.L. Libbert, I.K. Robinson, Phys. Rev. B 55 (1997) 13193.
[10] http://www.rontecusa.com/products.htm.
[11] K. Holldack, J. Feikes, W.B. Peatman, Nucl. Instrum. Methods A 467–468 (2001) 235.
[12] I.A. Vartanyants, I.K. Robisnon, Opt. Commun. 222 (2003) 29.
[13] W. Leitenberger, H. Wendrock, L. Bischoff, T. Weitkamp, J. Synchrotron. Radiat. 11 (2004) 190.
[14] K. Fezzaa, F. Comin, S. Marchesini, R. Coisson, M. Belakhovsky, X-ray Sci. Technol. 7 (1997) 12.
[15] S. Marchesini, K. Fezzaa, M. Belakhovsky, R. Coisson, Appl. Optics 39 (10) (2000) 1633.
[16] M. Born, W.E. Wolf, Principles of Optics, Seventh ed., Cambridge University Press, Cambridge, 1999.
[17] T. Geue, M. Schulz, J. Grenzer, U. Pietsch, A. Natansohn, P. Rochon, J. Appl. Phys. 87 (2000) 7712.